52st AIAA Aerospace Sciences Meeting
13 - 17 Jan 2014, National Harbor, MD
AIAA-2014-0319

Estimation of Aero-Optical Wavefronts Using Optical and Non-Optical Measurements

Robert Burns[1], Stanislav Gordeyev[2], Eric Jumper[3]
University of Notre Dame, Notre Dame, Indiana, 46545

Sivaram Gogineni[4],
Spectral Energies, LLC, Dayton, OH 45431

Michael Paul[5] and Donald J. Wittich[6]
Air Force Research Laboratory, Directed Energy Directorate, Kirtland AFB, NM 87117

In this paper we present two algorithms for estimating the aero-optical aberration of a transonic flow around a 2-D turret based on Malley probe signals or pressure signals from few selected points. These two algorithms use Artificial Neural Networks and Linear Stochastic Estimation of varying model orders to estimate Proper Orthogonal Decomposition modal coefficients. These estimated coefficients are then used to reconstruct an estimated wavefront. This estimated wavefront is subtracted from the true wavefront to obtain a simulated reduction in the overall level of optical aberration. Reductions of up to 48% are achieved for both models. A robustness analysis is also performed, in which it is found that the algorithm is not sufficiently robust to changing flow conditions. Solutions are proposed for further investigation.

I. Introduction

TURRETS are often used to send or transmit a laser beam from an airborne platform, as turrets provide convenient mechanical means to steer the laser beam. Also turrets are used in airborne imaging applications. However, its non-aerodynamic bluff-body shape creates a complex turbulent flow around it [1], and the resulting unsteady density fluctuations around the turret might impose detrimental aero-optical effects [2,3] on the incoming or outgoing beam at even low Mach number of 0.3. As these aero-optical effects result in unwanted unsteady beam defocus and jitter on the target, they might disrupt a high-speed optical link in free-space laser-based communication systems or might blur images taken using from airborne turrets.

When the flow is subsonic everywhere around the turret, essential flow features and related aero-optical distortions have being extensively studied in last few years and fairly well-understood [1,3-7]. But for incoming Mach numbers larger than approximately 0.55, the flow on top of the turret becomes locally supersonic, with a resulting local moving shock [1,5,8], with the shock extent and the angle depending on the incoming Mach number. The shock creates unsteady density gradients in the flow and promotes an earlier separation of the flow off the turret. All these shock-related features add additional strong aero-optical distortions to the outgoing beam [5,9,10].

Several ways to mitigate the aero-optic, shock-related problem has been recently demonstrated. One approach is to manipulate the flow using the flow control. The passive flow control utilizes a porous screen, which introduces total pressure losses near the surface of the turret and, as a result, slows the flow down to subsonic speeds, thus eliminating the unsteady shock [10]. The active flow control shows some promise in directly manipulating the shock [11].

---

[1]Graduate Student, Department of Aerospace and Mechanical Engineering, Hessert Laboratory for Aerospace Research, Notre Dame, IN 46556, AIAA Student Member.
[2]Research Associate Professor, Department of Mechanical and Aerospace Engineering, Hessert Laboratory for Aerospace Research, Notre Dame, IN 46556, AIAA Associate Fellow.
[3]Professor, Department of Mechanical and Aerospace Engineering, Hessert Laboratory for Aerospace Research, Notre Dame, IN 46556, AIAA Fellow.
[4]President, 5100 Springfield St. Suite 301, Dayton OH 45431, Senior AIAA Member.
[5]Aero-Optics Engineer, Laser Division, 3550 Aberdeen Ave SE.
[6]Aerospace Engineer, Laser Division, 3550 Aberdeen Ave SE.

An alternative approach, called an adaptive optics (AO) [12], does not (usually) modify the flow but rather measures the effective optical aberrations using direct measurements and cancels them imposing a conjugate wavefronts on the outgoing beam. This conventional adaptive optics technique is widely used in ground-based astronomy [12] to correct for low-frequency (~ 1 - 10 Hz) atmospheric-related distortions. As aero-optical aberrations are typically of much higher frequency (~1 – 5 kHz), latency issues in the feedback loop, related to measuring instantaneous wavefronts, make the traditional adaptive optics approach to be currently outside of capabilities of correcting adaptive-optical systems [13, 14].

As the main problem in applying the conventional AO to aero-optics is related to measuring wavefronts fast enough [13,15], several variations of AO approaches, which do not require direct wavefront measurements, have been recently investigated to address aero-optical mitigation. One of them, called an open-loop approach, relies on combining flow control and adaptive optics. It forces the flow to be predictable using flow regularization techniques [16], thus eliminating the need to measure instantaneous wavefronts, and uses a Phased-Locked Loop technique [13], to compensate for these known distortions.

A second variation of AO, instead of measuring wavefronts, estimates them from either optical input from very sparse array of sensors, or from non-optical input from several sensors. The non-optical input using surface pressure field to estimate aero-optical environment around turrets was investigated by Andino et al [17], in which POD was combined with surface pressure measurements to develop a closed-loop feedback controller. Controllers have also been developed with the goal of minimizing pressure fluctuations across a beam aperture in a pitching environment using active flow control [18].

This paper will focus on a way of estimating aero-optic flow disturbances using two estimation techniques: Proper Orthogonal Decomposition (POD) with an Artificial Neural Network (ANN) [19] and POD with Linear Stochastic Estimation (LSE). The input signals will be either optical or non-optical in nature. This is advantageous for two reasons: 1) in some cases, the target of a laser-based system may not provide a sufficiently strong return signal to drive a traditional closed-loop adaptive optic system and 2) it may be possible to significantly reduce the computational effort required for wavefront estimation if low-order modeling and relatively few and preferably analog sensors are used to estimate the flow state rather than very computationally-intensive Shack-Hartmann Wavefront Sensors.

In this paper, it is desired to build on these aero-optic mitigation strategies by investigating new techniques that make use of either optical or non-optical measurements to estimate instantaneous optical wavefronts. The techniques used in this paper will combine *a priori* knowledge of the flow's behavior with actual measurements to estimate the state of the flow. Eventually, an adaptive optics system could be built using the estimation techniques presented in this paper.

This technique was applied to the transonic flow around a two-dimensional turret. The flow around the two-dimensional turret was shown to have most essential flow features, as around three-dimensional turrets [1,20] and was found to provide a convenient platform to understand the nature of aero-optical distortions around turrets, as well as to test different flow mitigation approaches at subsonic speeds [21-23]. Chapter II provides a theoretical background and Chapter III describes the experimental set-up. Results of estimating aero-optical distortions from either optical (deflection angles) or non-optical (surface pressure) inputs are provided in Chapters IV and V, respectively. Conclusions are given in Chapter VI.

II. Theoretical Background

The purpose of this paper is to study the feasibility of an aero-optic wavefront estimator from optical or non-optical data. Similar to [17], it is proposed to first decompose wavefronts into Proper Orthogonal Modes, and then to train an estimation algorithm to obtain the modal coefficients from relevant optical or non-optical signals. Let the true state of the flow field at time step k be denoted as $\mathbf{y}_k$. The true state of the system evolves according to some non-linear vector-valued function $\mathbf{f}$,

$$\mathbf{y}_k = \mathbf{f}(\mathbf{y}_{k-1}) . \quad [1]$$

Let the true instantaneous optical path difference (OPD) of the flow field at time step k be denoted as $\mathbf{d}_k$. Measurements of OPD may be obtained using some measurement function $\mathbf{h}_{OPD}$ on the true flow state,

$$\tilde{\mathbf{d}}_k = \mathbf{h}_{OPD}(\mathbf{y}_k) . \quad [2]$$

Similarly, the input field (limited optical or surface pressure values) may be measured as

$$\tilde{\mathbf{p}}_k = \mathbf{h}_p(\mathbf{y}_k) . \quad [3]$$

The wavefronts estimated from measurements using the high-speed wavefront sensor are snapshots of $\tilde{\mathbf{d}}_k$.

The difficulty with using a direct wavefront feedback approach as it relates to adaptive optics is that much computational effort is required to reconstruct the wavefronts and full wavefront feedback may not always be possible in practical systems. However it is generally much easier to measure beam jitter at selected points or to measure the pressure field near the aperture. Therefore, it is desired to establish an empirical relationship between OPD and measurements of the optical/pressure field,

$$\hat{\mathbf{d}}_k = \mathbf{g}(\tilde{\mathbf{p}}_k, \tilde{\mathbf{p}}_{k-1}, \ldots, \tilde{\mathbf{p}}_{k-M}; \hat{\mathbf{d}}_{k-1}, \hat{\mathbf{d}}_{k-2}, \ldots, \hat{\mathbf{d}}_{k-M}) \quad [4]$$

where **g** is some non-linear function and *M* is the order of the model. One of the two approaches taken in this paper is to establish the non-linear function **g** by forming an artificial neural-network (ANN) and training this network using time-resolved observations of OPD and optical/pressure fields. Once the network is trained, it can then be used to estimate OPD using a concurrent measurement of the optical or pressure field and past estimations of the OPD field. Figure 1 shows the topology of the neural networks used in this paper. The algorithm shown in Figure 1 is a direct implementation of the function **g**. In this figure, *M* is the order of the system (number of past points used), *N* is the number of outputs, and *L* is the number of spatial points where inputs were measured. The first stage of the loop takes in the most recent *M* estimations of the POD coefficients and inputs. These coefficients are then weighted by the matrices $\mathbf{W_1}$ and $\mathbf{W_2}$, and are then added together with a bias matrix $\mathbf{b_1}$. It should be noted that up to this point, the neural network is very similar to Linear Stochastic Estimation and will be examined later in the paper as well. The weighted inputs are now fed into activation functions, which are typically sigmoid in nature. The choice of activation function often used in neural networks is the hyperbolic tangent. This choice is made because the hyperbolic tangent is defined over the domain of real numbers, but is bounded asymptotically on the interval [-1, 1]. It is this choice of activation function that gives the neural network its nonlinear character and makes it distinct from LSE. The outputs of activation layer are then passed into a final output layer, which is a simple linear transformation. The outputs of this layer are the estimation of the current POD coefficients. These coefficients are then fed back into the input layer on the next iteration, thereby completing the feedback loop. The training objective is then the error between the predicted coefficients and the measured coefficients based on a sequence of training inputs. This objective is minimized using the Levenberg-Marquadt algorithm. MathWorks' MATLAB Neural Network Toolbox was used to perform the optimization.

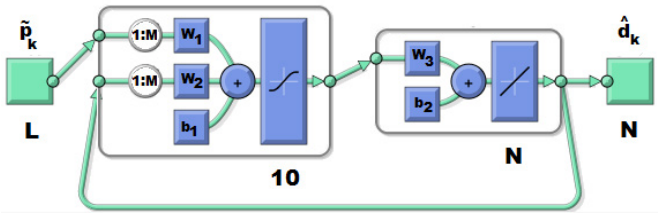

Figure 1: Neural network topology

The aforementioned approach will allow OPD to be estimated from the optical/pressure field, but direct implementation of this scheme would be extremely computationally intensive. A better approach is to use Proper Orthogonal Decomposition to reduce the required dimensionality of the model.

The objective of Proper Orthogonal Decomposition [24] in the scalar case is to approximate a function, $z(x,t)$ over some domain as a linear combination of temporal coefficients $a_k(t)$ and spatial modes, $\varphi_k(x)$ as

$$z(x,t) \approx \sum_{k=1}^{M} a_k(t)\varphi_k(x). \quad [5]$$

Furthermore, if orthonormality is imposed on the basis functions as

$$\int_X \varphi_m(x)\varphi_n(x)dx = \delta_{mn}, \quad [6]$$

then the temporal coefficients may be calculated as

$$a_k(t) = \int_X z(x,t)\varphi_k(x)dx. \quad [7]$$

The problem of calculating POD modes in the multi-dimensional case for discrete-time data is typically solved using the singular-value decomposition (SVD). In our case, let **V** be a matrix of measurement snapshots of the OPD organized by column vectors of samples ordered by increasing time as shown

$$\mathbf{V} = \begin{bmatrix} \tilde{\mathbf{d}}_1 & \tilde{\mathbf{d}}_2 & \cdots & \tilde{\mathbf{d}}_N \end{bmatrix}. \quad [8]$$

Then **V** may be decomposed using SVD as

$$\mathbf{V} = \mathbf{U}\boldsymbol{\Sigma}\mathbf{W}^{H}, \quad [9]$$

and the spatial modes may be extracted from the columns of **U**,

$$\mathbf{U} = \begin{bmatrix} \boldsymbol{\varphi}_1 & \boldsymbol{\varphi}_2 & \cdots & \boldsymbol{\varphi}_N \end{bmatrix}. \quad [10]$$

The temporal coefficients are then calculated from a projection of the spatial modes onto the original observations.

$$\mathbf{a} = \mathbf{U}^{+}\mathbf{V} \quad [11]$$

The modes are ranked by the importance of their contribution to the overall energy of the system. Quite often, the POD modes converge quickly to give a good low-dimensional model. This is especially true when very dominant flow structures are present, such as shocks. This approach allows the modes to be determined *a priori*, so that the model may be trained to estimate the modal coefficients rather than the entire OPD field.

Linear Stochastic Estimation (LSE) LSE will be used as a baseline model with which to compare the ANN approach. As discussed previously, the LSE approach is essentially equivalent to the first stage in the ANN algorithm. The variation of LSE used in this paper seeks to determine the **A** and **B** matrices of a discrete linear system,

$$\hat{\mathbf{d}}_k = \mathbf{A}\begin{bmatrix} \hat{\mathbf{d}}_{k-1} \\ \hat{\mathbf{d}}_{k-2} \\ \vdots \\ \hat{\mathbf{d}}_{k-M} \end{bmatrix} + \mathbf{B}\tilde{\mathbf{p}}_k. \quad [12]$$

where the tilded quantities are physical measurements such as pressure or Malley probe signals, and the hatted quantities are estimations of the POD coefficients of the system. In this way, we make the careful distinction between measurements and estimations. LSE seeks to find the **A** and **B** matrices subject to the minimization objective,

$$\left[\mathbf{A}, \mathbf{B}\right] = \underset{\mathbf{A}\in\mathbf{R}^{NxNM},\mathbf{B}\in\mathbf{R}^{NxL}}{\arg\min} \sum_{k=M+1}^{K} \left\| \hat{\mathbf{d}}_k - \tilde{\mathbf{d}}_k \right\|, \quad [13]$$

where M is the order of the system, N is the number of outputs, L is the number of inputs and the norm, $\|\cdot\|$, is the Euclidian or the L^2-norm. The matrices may therefore be easily obtained using an optimization algorithm such as gradient descent.

III. Experimental Setup and Flow Regimes

To investigate aero-optical effects at transonic speeds around the cylindrical turret, a turret with a conformal window was designed and manufactured, as shown in Figure 2. The turret is 98 mm long with a 104 mm diameter. The turret has a built-in set of optical elements, consisting of two off-the-shelf cylindrical lenses and a flat mirror, designed to reflect an incoming collimated beam with a minimum amount of optical distortions; that is, optically it is equivalent to an optical flat mirror. The optical aperture size is 30 mm x 50 mm. The outer curvature of the front cylindrical lens matches the curvature of the cylindrical turret. Nine unsteady pressure sensors, shown in Figure 2, right, were mounted in the turret allowing the simultaneous acquisition of an unsteady pressure field and optical wavefronts.

The cylindrical cylinder was tested in a test section with a back-step; this test section has a height jump, from 4” to 6”, at the location of the partially-protruding cylinder, see Figure 3 for schematics of the test section. The cylinder protrusion was 7.5 mm, relative to the upstream bottom tunnel wall.

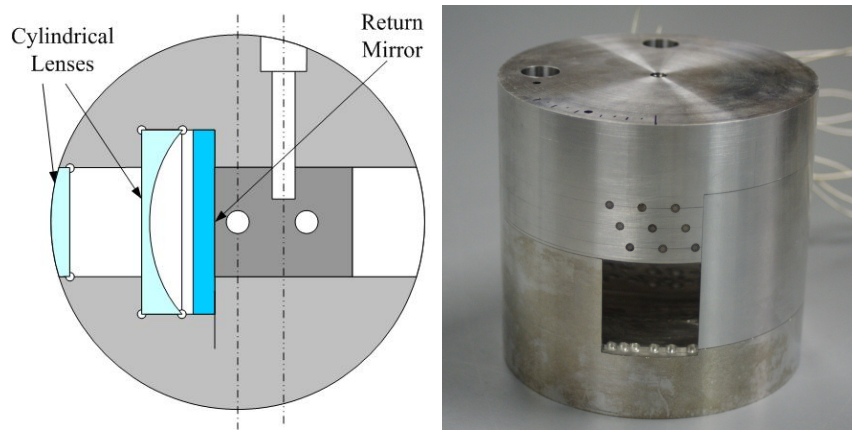

Figure 2: Cylindrical turret with a conformal window: drawing (left) and picture (middle). Right picture: an additional conformal turret with embedded unsteady pressure sensors.

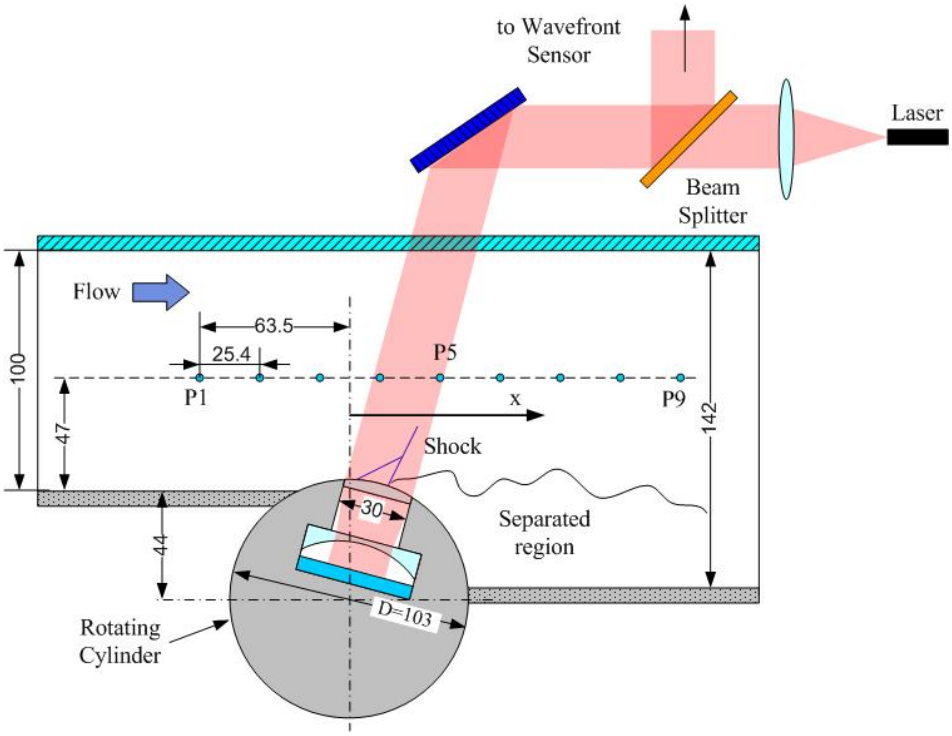

Figure 3: Schematic of the optical set-up.

Optical measurements were performed with a high-speed Shack-Hartmann wavefront sensor, see Figure 3, for the optical set-up. The sensor sampling rate was 10 kHz with the spatial resolution of 54x32 subapertures, with 54 subapertures in the streamwise direction. The camera was synchronized with a data acquisition system that sampled the 9 Kulite pressure sensors on the surface of the turret at 50kHz. Aero-optical measurements were collected at several elevation angles and different incoming transonic speeds. Figure 4 shows a schematic of the test configuration using the modified turret with unsteady pressure sensors (Kulites). A Schlieren system was used to visualize the location and the strength of the local shock on top of the partially-protruding cylinder, as shown in Figure 5. The test section was also equipped with 8 static pressure ports to monitor the streamwise evolution of the flow speed in the test section.

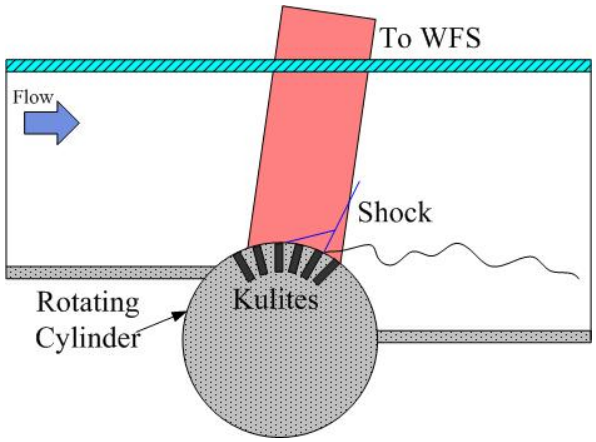

Figure 4: Schematic of Simultaneous Pressure-Wavefront measurements

Investigation of the flow around the partially-protruding cylinder had revealed that the flow features strongly depend on the incoming Mach number. Figure 5 shows time-averaged Schlieren images for several different Mach numbers [10]. The baseline shock dynamics were found to be quite sensitive to the local speed over the cylinder, displaying both unsteady and nearly-steady characteristics.

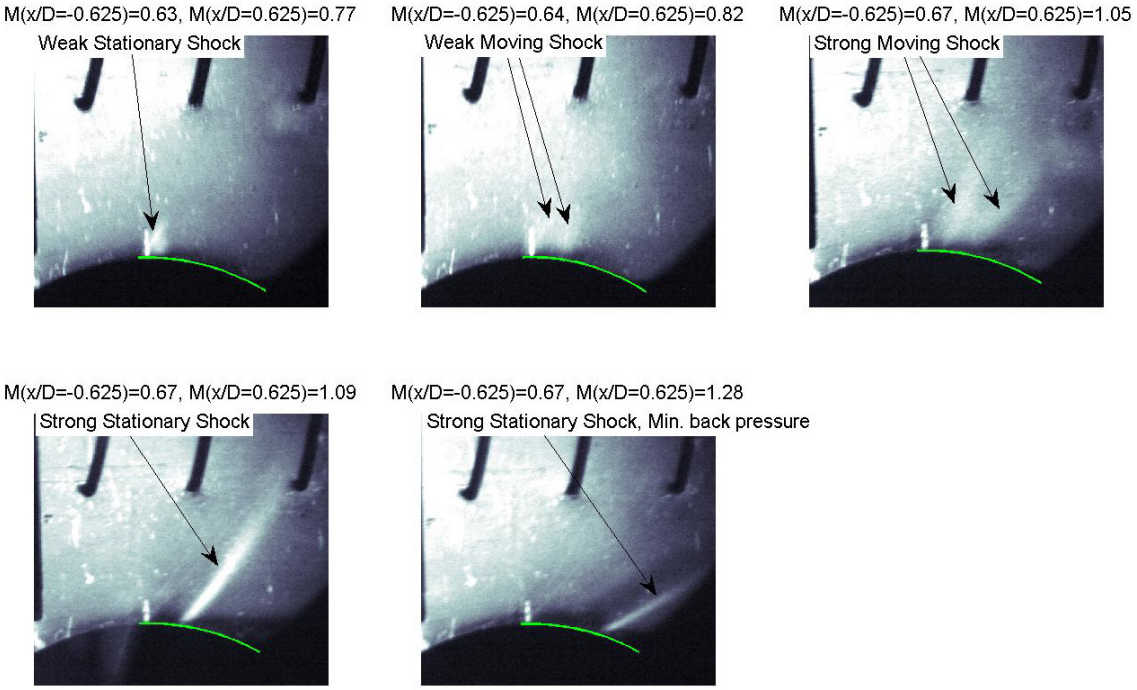

Figure 5: Schlieren flow visualization for different flow regimes. The outline of optical aperture is labeled by a green line. From [10]

The shock location and evolution at different flow regimes was measured using high-speed shadowgraph. Representative pictures of the shock at different times for the weak moving shock case are shown in Figure 6. In this flow regime, the shock forms upstream, gains the strength and moves upstream over the aperture in almost periodic fashion. Very similar shock dynamics was reported over 3-D turret at transonic speeds [25]. For demonstration purposes, only the weak shock case was considered in the paper.

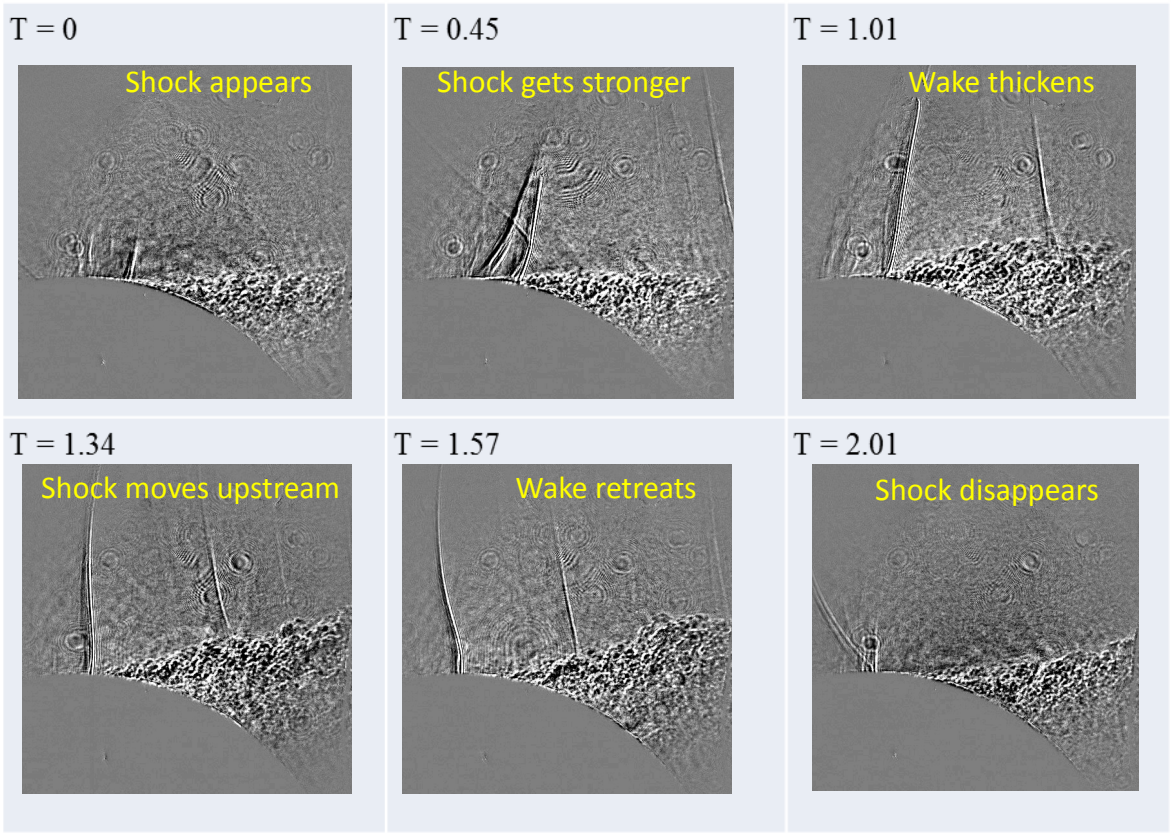

Figure 6: Shock temporal evolution for the weak moving shock case. M = 0.65 (x/D = - 0.625), M = 0.83 (x/D = 0.625)

A sample of synchronized pressure and wavefront data is shown in Figure 7. The middle of the aperture was located at the elevation angle of 105 degrees. The elevation angle is measured from the upstream direction. As the wavefronts were mostly spanwise-uniform, 1-dimensional, tilt-removed wavefronts slices in the streamwise direction were extracted and plotted as a function of the elevation angle and time in Figure 7, left plot. The presence of the shock, which creates the discontinuity in the wavefront, is labeled by a thick black arrow during one cycle. Consistent with shadowgraph snapshots in Figure 6, the shock-related wavefront discontinuity is formed around 110 degrees, the wavefront discontinuity moves upstream and eventually disappears near 95 degrees. Simultaneous time-evolution of surface pressure at 9 points are presented in Figure 7, left plot. It is clear that there is a very periodic behavior in both the pressure signals and the wavefront evolution. There is a small phase delay between pressures and wavefronts, related to the inertia of the separated wake. The shock frequency is approximately 1kHz, so the chosen acquisition rate of 10kHz provides good temporal resolution for resolving the motion of the shock.

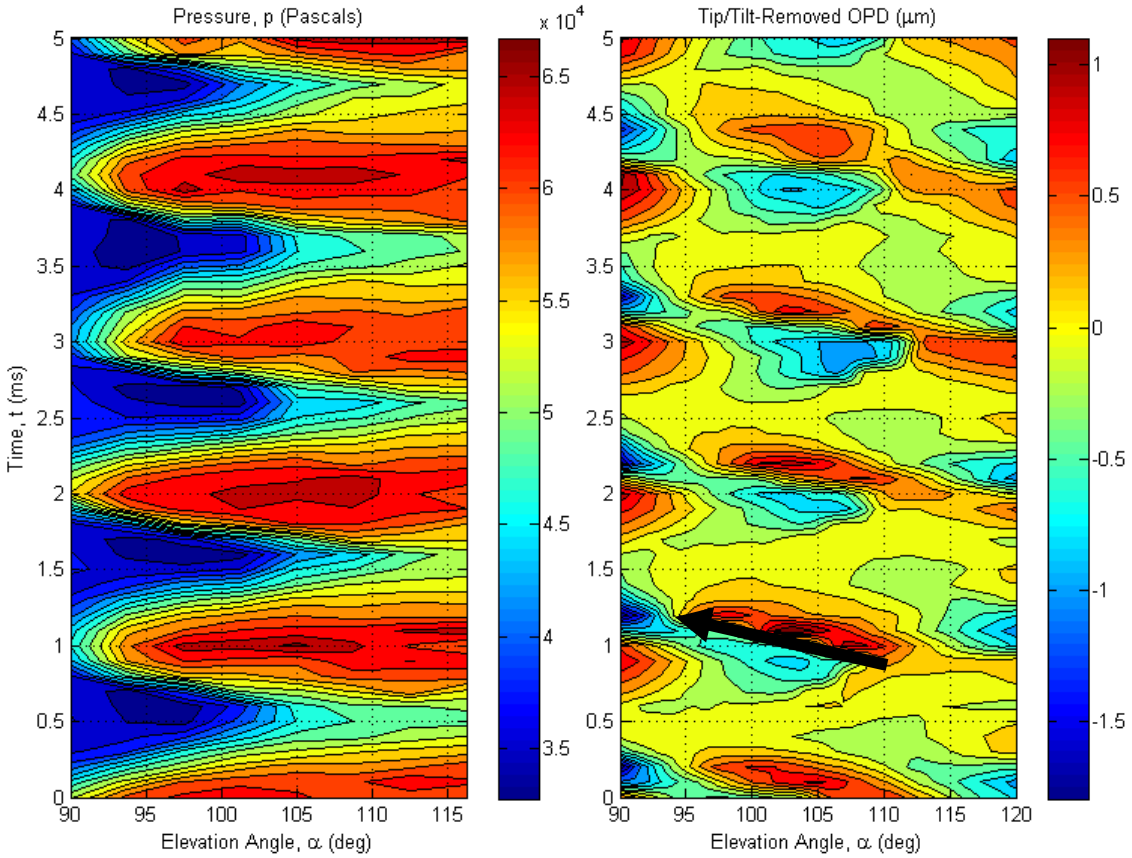

Figure 7: Synchronized pressure (left) and 1-d slices of wavefront (right) measurements. The shock is labeled as a thick black arrow.

IV. Results from Simulated Malley Probe/Wavefront Experiments

The ANN estimation approach was applied to the transonic wavefront data in conjunction with two simulated Malley beams. The simulated Malley beam was obtained by extracting the wavefront slope from wavefront data at elevation angles of 95 degrees and 105 degrees. This was done to test the feasibility of this method before performing a more extensive experiment and analysis with simultaneous pressure and wavefront measurements.

The neural network was trained over 4000 samples, and then it was used to estimate the next 100 using only the network itself and the input wavefront slopes, θ_1 and θ_2. The results of the estimation algorithm are shown in Figure 8. An overall reduction in OPD_{rms} of 22% could be achieved using this method. An example of the reconstruction estimate is shown in Figure 9. A major challenge in using the Malley Probe as a training signal is that it is very noisy. Additionally, it is not clear from the analysis that there is a strong connection between the Malley Probe signals used and the highest-energy POD mode coefficients, which is critical to the performance of this type of estimation system. If the estimation window is extended from 100 samples to something significantly larger, the estimation system will lose its "lock" on the phase of the signal and will actually amplify the effective OPD.

The conclusion drawn from this preliminary analysis was that a cleaner input signal is needed to obtain a better estimation of the POD modes. The type of sensor chosen to provide a better training signal was a Kulite pressure sensor, and the results from that experiment are presented in the next section.

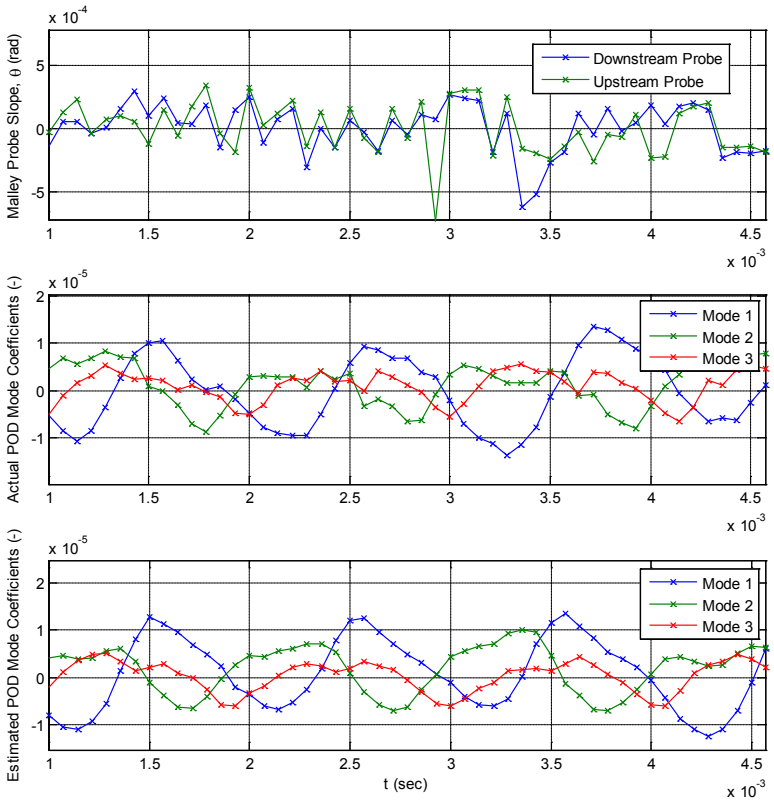

Figure 8: Modal coefficient estimation from Malley probe beams

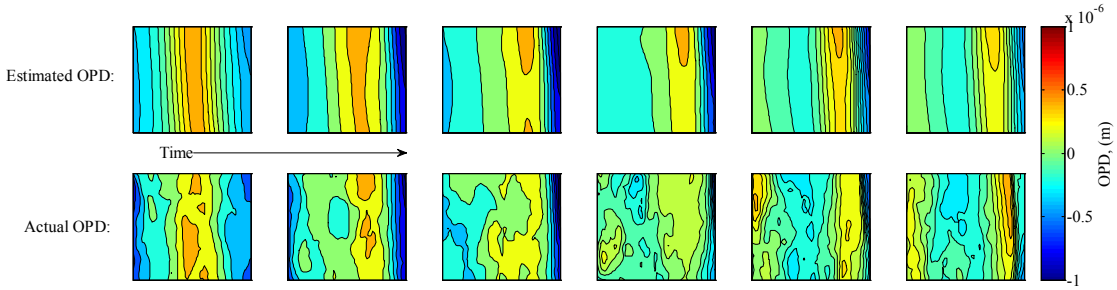

Figure 9: Comparison of estimated and actual wavefronts

V. Results from Simultaneous Pressure/Wavefront Experiment

The first three POD modes of the synchronized pressure/wavefront data are shown in Figure 10. These three modes contain 93% of the energy in the flow. Therefore, a very high level of reduction in effective OPD_{rms} is possible if these three modes are accurately estimated and optically controlled.

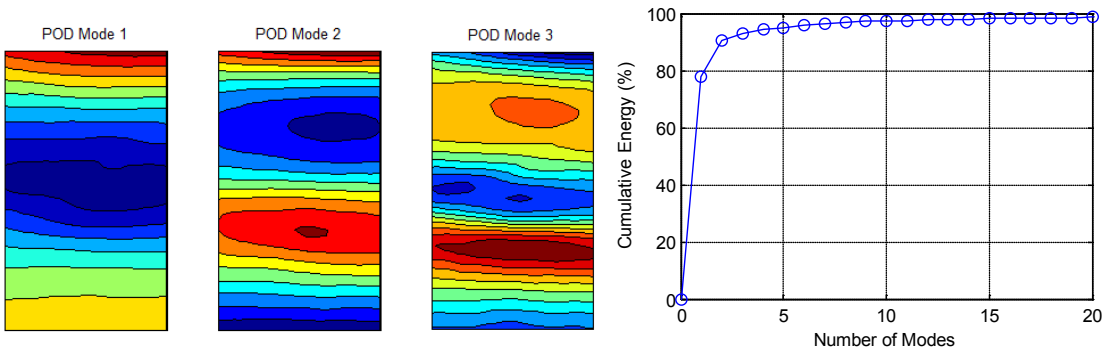

Figure 10: First three POD modes, containing 93% of the energy of the flow

The LSE and ANN algorithms were tested for four different model orders to determine the effect of model order on accuracy of estimations. In the case of the ANN, the model order is the number of previous inputs used, called tap delays. In the case of LSE, the model order refers to the number of previous states that were estimated. Both models were trained over 1000 samples of data, and then used to estimate the next 1000 samples. The initial conditions for each estimator are always set to 0, which does have the effect of introducing start-up transients that last for a few cycles of shock motion. The locations of the pressure signals were at elevation angles of 94 degrees, 101 degrees, and 108 degrees. These were chosen to be evenly spaced and cover a large part of the total aperture. The pressure training signals are shown in Figure 11. These signals are much cleaner than the Malley Probe signals, shown in Figure 8, top plot, and are related to the motion of the shock, as discussed in Figure 7.

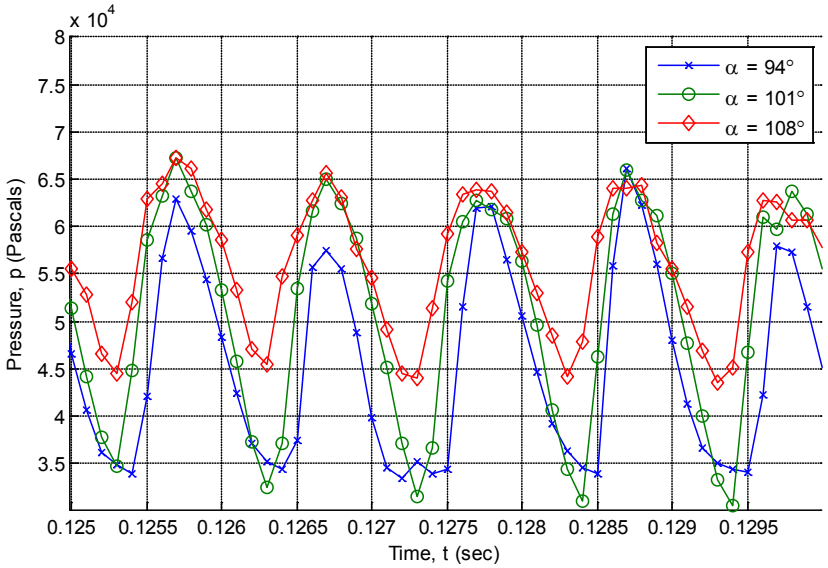

Figure 11: Pressure training signals

A simulation was performed to compare the baseline case with the Neural Network and Linear Stochastic Estimation methods for 1st, 2nd, 3rd, and 4th-Order models. The results of this simulation are shown in Figure 12. These results were obtained by subtracting the estimated wavefronts from the actual aberrations, and then normalizing these residual time-averaged values by the mean uncorrected level of OPD_{rms}. The ANN accuracy increases by a total of 9% from the single-delay network to the 4-delay network. The LSE accuracy takes a much larger jump from the first-order model to the third-order model for an accuracy jump of almost 25%. The 4th-order LSE actually does a slightly worse job than the 3rd-order variant, meaning that it is near this point that the linear algorithm begins to become overtrained and loses some robustness to changing flow conditions. It would not be advisable to go significantly beyond a 4th-order method, as the algorithm will become much less robust to changing flow conditions as the order of the model increases. Generally, the order of the model will increase the accuracy but reduce the robustness. This assertion will be discussed further later in this section.

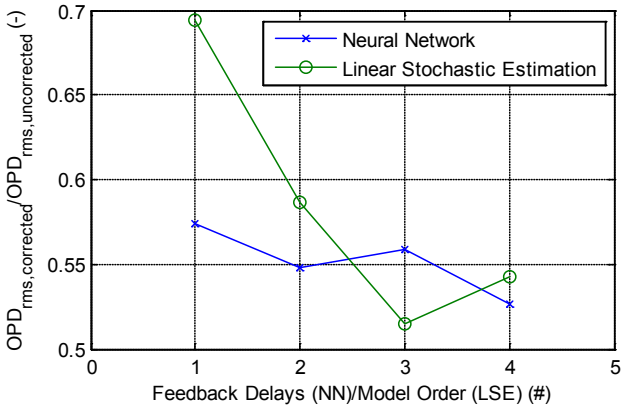

Figure 12: OPD_{rms} Reduction Obtained in the Weak Shock Case

Since the 3rd-order model gave good results for both the ANN and LSE cases, this topology was selected for individual analysis. The results of the coefficient estimation are shown in Figure 13. Tracking for the first two modes is very good in both algorithms. The majority of the energy in this transonic flow is contained in these first two modes, so a very large portion of the contribution to the overall reduction in OPD_{rms} is obtained from these modes. Tracking the third mode proves to be the most challenging due to its more complex dynamics; however, the estimator still helps more than it hurts in this case. Naturally, tracking additional modes would help the overall reduction in optical aberration if these modes can be estimated accurately. However, since a significant reduction in the quality of the estimation is observed in the third mode, estimation of higher order modes would not be advisable in the current iteration of this algorithm.

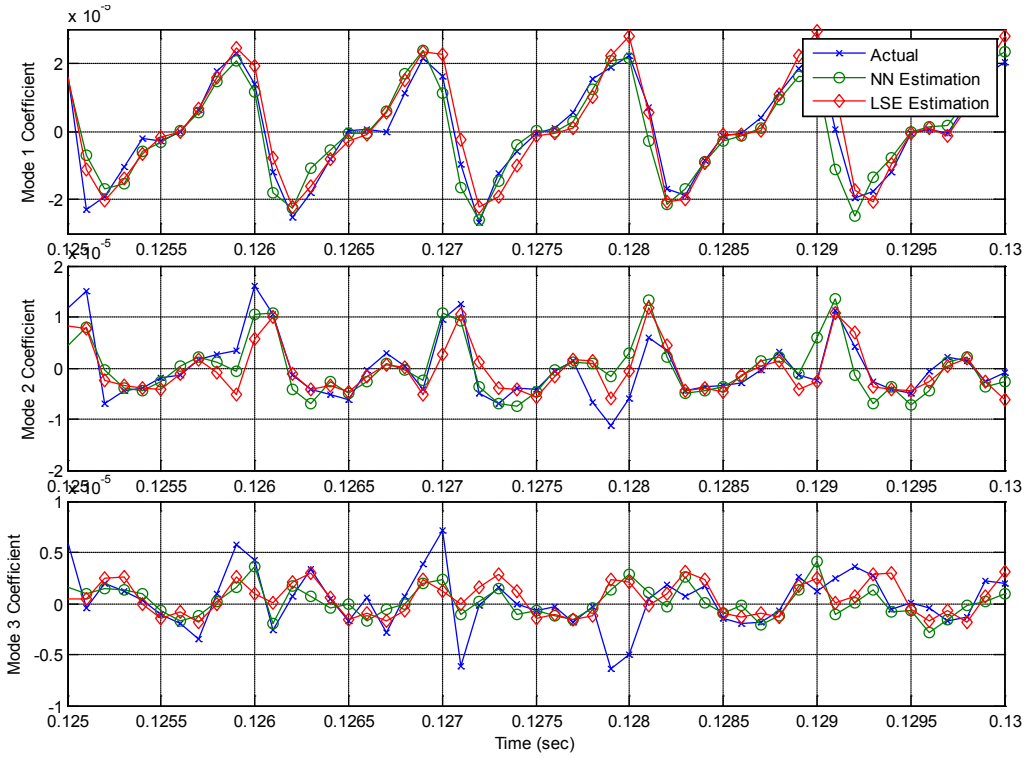

Figure 13: LSE and ANN estimation of the first three POD modes using third-order estimation models

The instantaneous reduction in OPD_{rms} that could be achieved by imposing the conjugate of the estimated aberration on an outgoing beam is presented as a function of time in Figure 14. The mean reduction achieved for the

neural network estimator is 44%. The mean reduction for the linear stochastic estimator is 48%. Over this window, it is important to note that the estimation model never makes the effective OPD significantly worse than the uncorrected case. Note also that there is an apparent floor of approximately 0.2 $OPD_{rms,corrected}/OPD_{rms,uncorrected}$ (see Figure 14) beneath which the algorithm can no longer reduce the effective aberration. These low-OPD time intervals are related to times where the shock was not present over the turret. Therefore, only higher-order modes in the wavefront/pressure signals were present, which was beyond the first three POD modes that the algorithm attempts to estimate. A higher-order model would be needed to further reduce this lower threshold.

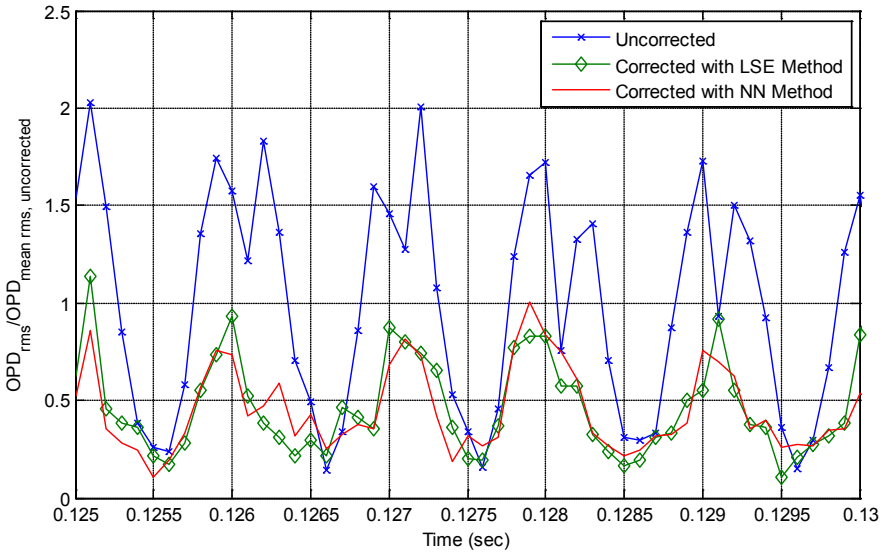

Figure 14: OPD_{rms} reduction for 3rd order LSE and NN methods

While the mean OPD_{rms} improvement is very important for applications such as directed energy, laser-based communications systems are more sensitive to short-interval dropouts stemming from spikes in the OPD. To measure this effect, the probability distribution functions for instantaneous OPD_{rms} were computed for the baseline, NN-corrected, and LSE-corrected cases. The results are shown in Figure 15. The probability or frequency of large-amplitude spikes is greatly reduced with all of the models. This would be highly beneficial to free-space laser communication systems since the frequency of large-OPD-related interruptions would be reduced, thus reducing the need to retransmit interrupted or corrupted data packets.

Additional parameters were also investigated as part of this work. Besides varying the number of tap delays, the sensitivity of the estimation algorithms to the number of input signals and changing flow conditions was also studied. For the remainder of this section, we will discuss an analysis of the linear stochastic estimator since both the neural network and the linear stochastic estimator performed similarly and the mathematics are simpler in the LSE case. We will propose methods for improving both the ANN and the LSE approach.

In the case of varying number of input signals, it may be seen from that the signals in question are nearly linearly combinations of one another. From this, it can easily be shown that there is a manifold of **B** matrices in the LSE algorithm (to within a small threshold, in a least-squares sense) that adequately fit the training data, and the number of these matrices grows with number of additional inputs. It was found by trial-and-error that 2 inputs were sufficient to estimate the state of the flow, while adding more inputs did not significantly help or hurt the performance of the algorithm. In the case of the Malley probe, additional inputs actually hurt the performance of the algorithms due to the additional input of noise into the system.

The robustness of the approach was also examined for both longer-time predictions as well as changing flow conditions. It was found that both approaches had difficulty tracking the modal coefficients for both longer quasi-steady runs as well as deliberate but incremental changes in the flow conditions. In the former case, the problem is not the issue of time *per se,* but rather natural changes occurring in the tunnel conditions due to slow drifts in incoming flow conditions. Shock dynamics are very sensitive to external pressure gradients, and it is difficult to control them tightly. It is clear from this that the robustness of the approach needs improvement.

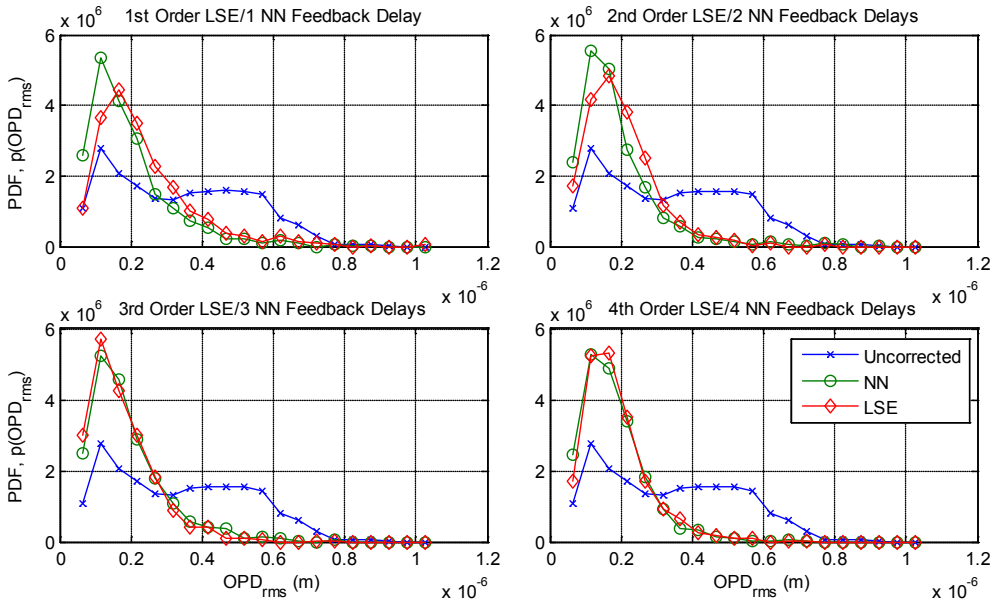

Figure 15: Comparison of uncorrected and corrected probability density functions for both estimation methods for varying model orders.

To better understand the robustness of the LSE model, it is helpful to consider the degenerate case of the model: the zeroth-order case, where the estimation of the coefficients is solely determined by the current-only input pressures and the **B** matrix in Eq. 12. If the POD coefficients could be well-approximated as a linear combination of the inputs, then in a sense the degenerate case would be the most "robust" since small frequency changes in the true POD coefficients would be physically reflected in the pressure inputs and therefore would also be well-approximated by the POD coefficient estimation. However, the degenerate case is simply insufficient to capture the dynamics of the system and some past information is needed to predict it accurately. One can conclude from this argument that in general lower-order models will tend to be more robust, while higher-order models will tend to be more accurate.

This conclusion, while a good guiding principle, is still an oversimplification of the true problem. As previously mentioned, there could be a manifold of solutions for the **A** and **B** matrices in Eq. 12 that give good estimations for well-behaved experimental data. The question is then clearly: is there a selection of **A** and **B** that compromises a small amount of accuracy for additional robustness? The solution could be provided by extending the model with a robustness parameter or by cross-training the model on multiple sets of data, each perturbed by some small change in the imposed pressure gradient.

In order to include a robustness parameter, one could extend the linear stochastic estimator model given by Eq. 12 to be in state-space form as follows,

$$\begin{bmatrix} \hat{\mathbf{d}}_k \\ \hat{\mathbf{d}}_{k-1} \\ \vdots \\ \hat{\mathbf{d}}_{k-M+1} \end{bmatrix} = \begin{bmatrix} \mathbf{A}_{N\times N(M-1)} & \mathbf{A}_{N\times N} \\ \mathbf{I}_{N(M-1)\times N(M-1)} & \mathbf{0}_{N(M-1)\times N} \end{bmatrix} \begin{bmatrix} \hat{\mathbf{d}}_{k-1} \\ \hat{\mathbf{d}}_{k-2} \\ \vdots \\ \hat{\mathbf{d}}_{k-M} \end{bmatrix} + \begin{bmatrix} \mathbf{B} \\ \mathbf{0}_{N(M-1)\times L} \end{bmatrix} \tilde{\mathbf{p}}_k \,. \qquad [14]$$

For convenience, we will denote the augmented **A** matrix as $\mathbf{A}_{\mathbf{aug}}$ and the augmented **B** matrix as $\mathbf{B}_{\mathbf{aug}}$. The advantage of performing this augmentation is that the eigenvalues and z-plane transfer functions can now be extracted from the system. The eigenvalues of $\mathbf{A}_{\mathbf{aug}}$ give the dependency of future estimations based on past estimations. By minimizing the norm of the eigenvalues (with some weighting factor), the effect of prior estimations will decay more rapidly and more importance will be placed on the pressure inputs. This would improve the robustness of the estimator since it would respond more rapidly to frequency changes in the flow. Thus, the proposed improved objective function, Eq. 13, is

$$[\mathbf{A},\mathbf{B}] = \underset{\mathbf{A}\in\mathbf{R}^{NxNM},\mathbf{B}\in\mathbf{R}^{NxL}}{\arg\min} \sum_{k=M+1}^{K} \left\| \hat{\mathbf{d}}_k - \tilde{\mathbf{d}}_k \right\| + \mathbf{Q}\boldsymbol{\lambda}_{\mathbf{A}_{\mathbf{aug}}}, \quad [15]$$

where $\mathbf{Q}$ is a weighting matrix and $\boldsymbol{\lambda}_{\mathbf{Aaug}}$ is a column vector of the eigenvalues of the augmented A matrix. The challenge with this approach would be determining an appropriate weighting matrix. It is proposed that future work not only attempt this modification to the model, but examine the effect of the weighting matrix and develop good practices for choosing it.

In the case of the neural network-based approach, it is likely that the best option to increase robustness is to simply add additional sets of training data. Care should be taken to slightly vary flow parameters such as the amplitude and frequency of flow features contained in POD modes without fundamentally changing the flow regime. In an estimation system that uses either LSE or ANN, there is a domain of inputs within which the estimator should be stable and robust. If the flow conditions deviate outside this predefined region, an appropriate technique would be to retrain the model. Put another way, the models should be robust to nearly-linear changes in frequency and amplitude. Changes to flow topology should be handled by different training sets.

One of the major drawbacks with "blackbox" approaches such as neural networks is that it is much more difficult to extract meaningful physics from the model. In the case of the LSE, it is easier to relate things like eigenvalues to physical phenomena. It is proposed that future work continue to develop the augmented LSE model in parallel with the neural network model. Additionally, future work should examine the viability of support vector machines (SVMs) to replace the neural network model. ANNs may suffer from a solution that is located at a local minimum; however, SVMs will attempt to find the globally optimal solution. Perhaps worse than the drawback itself is that it is not always apparent when a non-globally minimal solution has been found in the ANN. Therefore, for the purposes of verification alone it is recommended that support vector machines be studied further in the application of flow estimation and prediction.

VI. Conclusions

Shock-induced aero-optical aberrations around turrets at transonic flow regimes are a significant obstacle to the implementation of laser transmission devices on airborne platforms. In order to successfully transmit a beam from an airborne platform flying at transonic speeds, it is necessary to implement some form of aero-optic mitigation strategy. There are currently three general strategies for aero-optic mitigation: passive flow control, active flow control, and adaptive optics approaches. In this paper, we present methods that could be integrated into an adaptive-optics control loop. The methods rely on small-beam Malley probe or pressure inputs that are then directly related to output wavefronts. This is advantageous in environments where a return beam is not present for a closed-loop adaptive optics sensor, in addition to avoiding the necessity to reconstruct complex wavefronts in real-time.

In this paper, we have presented two approaches that are closely related to one another. These models take advantage of regular features in the flow combined with measurements of related physical quantities to estimate Proper Orthogonal Modes of the Optical Path Difference in the flow field. One method of estimation is based on Linear Stochastic Estimation and the other method is based on the usage of Artificial Neural Networks. Both models were trained to predict POD mode coefficients from external sensor inputs. Two types of sensor inputs were used: simulated Malley Probe beams and synchronized pressure inputs. The LSE approach reduced aero-optical aberrations by up to 48% and the ANN approach reduced the aberrations by up to 46%. It was found that the NN approach gave a better estimation for lower model order while the LSE approach was able to achieve the best overall performance.

While the accuracy of the models for the given cases was good over a short temporal horizon, the models gave erroneous predictions as the flow field characteristics changed over time. It is proposed that future work focus on extending the LSE model to include a term in the minimization objective function to reduce the magnitude of the eigenvalues of the estimator. The effect of this change will be to reduce dependency on past observations and place more weight on input measurements, thereby speeding up the response of the system to changing flow conditions. It is also proposed that the ANN be trained with several slightly dissimilar sets of data, reducing overall accuracy of the model but allowing for some variation in frequency and amplitude of the POD coefficients. Finally, it is proposed that Support Vector Machines be investigated as an alternative to ANNs, as they do not suffer from the problem of giving locally but not globally optimal solutions.

Acknowledgments

This work was funded by the Air Force Research Laboratory, Directed Energy Directorate. The U.S. Government is authorized to reproduce and distribute reprints for governmental purposes notwithstanding any copyright notation thereon.

The authors also wish to thank Nicholas De Lucca for helping in collecting unsteady pressure data and Alexander Vorobiev for providing instantaneous shadowgraph movies.

References

[1] S. Gordeyev and E. Jumper, "Fluid Dynamics and Aero-Optics of Turrets", *Progress in Aerospace Sciences*, **46**, (2010), pp. 388-400.

[2] Gilbert, K. G. and Otten L. J. (eds), "Aero-Optical Phenomena," *Progress in Astronautics and Aeronautics*, Vol. 80, pp. 1-9, AIAA, New York, 1982.

[3] M. Wang, A.Mani and S. Gordeyev,"Physics and Computation of Aero-Optics", *Annual Review of Fluid Mechanics*, Vol. **44**, pp. 299-321, 2012.

[4] C. Porter, S.Gordeyev, M. Zenk and E. Jumper, "Flight Measurements of Aero Optical Distortions from a Flat-Windowed Turret on the Airborne Aero-Optics Laboratory (AAOL)", AIAA Paper 2011-3280, 2011.

[5] N. De Lucca, S. Gordeyev and E. Jumper, " The Airborne Aero-Optics Laboratory, Recent Data", Acquisition, Tracking, Pointing, and Laser Systems Technologies XXVI, Proceedings of SPIE, Volume 8395, Paper 8395-7, June, 2012.

[6] B. Vukasinovic, A. Glezer, S.Gordeyev, E. Jumper and V. Kibens, "Hybrid Control of a Turret Wake," *AIAA Journal*, Vol. **49**, No. 6, pp. 1240-1255, 2011.

[7] M. Palaviccini, L. Cattafesta and B. George," Passive Flow Control over a Three-Dimensional Turret with a Flat Aperture", AIAA Paper 2011-3265, 2011.

[8] Fang, S., Disotell, K. J., Long, S. R., Gregory, J. W., Semmelmayer, F. C., and Guyton, R. W., "Application of Fast-Responding Pressure-Sensitive Paint to a Hemispherical Dome in Unsteady Transonic Flow," *Experiments in Fluids*, Vol. **50**, No. 6, 2011, pp. 1495-1505.

[9] B. Vukasinovic, A. Glezer, S. Gordeyev, E. Jumper and V. Kibens, **"**Active Control and Optical Diagnostics of the Flow over a Hemispherical Turret**"**, AIAA Paper 2008-0598, 2008.

[10] S. Gordeyev, R. Burns, E. Jumper, S. Gogineni, M. Paul, and D. Wittich. "Aero-Optical Mitigation of Shocks Around Turrets at Transonic Speeds Using Passive Flow Control", AIAA Paper 2013-0717.

[11] B. Vukasinovic, A. Gissen, A. Glezer and S. Gogineni, "Fluidic Control of Transonic Shock-Induced Separation", AIAA Paper 2013-0529, 2013.

[12] R. Tyson, *Principles of Adaptive Optics*, Academic Press, 2nd edition, 1997.

[13] A. Nightingale, B. Goodwine, M. Lemmon, and E. Jumper, "Phase-Locked-Loop Adaptive-Optic Controller and Simulated Shear Layer Correction", AIAA Journal, Vol. **51**, No. 11, pp. 2714-2726, 2013.

[14] D. Duffin, "Feed-Forward Adaptive-Optic Correction of a Weakly-Compressible High-Subsonic Shear Layer", PhD Thesis, University of Notre Dame, 2009.

[15] A. Nightingale, B. Mitchell, B. Goodwine and E. Jumper, "Feedforward Adaptive-Optic Mitigation of Aero-Optic Disturbances", AIAA Paper 2008-4211, 2008.

[16] R. Rennie, D. Duffin and E. Jumper, "Characterization and Aero-Optic Correction of a Forced Two-Dimensional Weakly-Compressible Subsonic Free Shear Layer", *AIAA Journal*, Vol. **46**, No. 11, pp. 2787-2795, 2008.

[17] M. Andino, R. Wallace, and M. Glauser, "Boundary Feedback Flow Control: Proportional Control with Potential Application to Aero-Optics", *AIAA Journal*, Vol. **49**, No. 1, pp. 32-40, 2011.

[18] R. Wallace, P. Shea, and M. Glauser, "Simulation-Guided, Model-Based Feedback Flow Control for a Pitching Turret", AIAA Journal, Vol. **50**, No. 8, pp. 1685-1696, 2012.

[19] G. Cybenko, "Approximation by Superpositions of a Sigmoidal Function", *Mathematics of Control, Signals, and Systems*, Vol. 2, No. 4, pp. 303-314, 1989.

[20] S. Gordeyev, J.A. Cress, E. Jumper and A.B. Cain, "Aero-Optical Environment Around a Cylindrical Turret with a Flat Window", *AIAA Journal*, Vol. **49**, No. 2, pp. 308-315, 2011.

[21] S. Gordeyev, E. Jumper, T. Ng and A. Cain, **"**The Optical Environment of a Cylindrical Turret with a Flat Window and the Impact of Passive Control Devices**"**, AIAA Paper 2005-4657, 2005.

[22] S.Gordeyev, J. Cress, A. Smith and E. Jumper, **"**Improvement in Optical Environment over Turrets with Flat Window Using Passive Flow Control**"**, AIAA Paper 2010-4492, 2011.

[23] K. Wang, M. Wang, S. Gordeyev and E. Jumper "Computation of Aero-Optical Distortions over a Cylindrical Turret with Passive Flow Control", AIAA Paper 2010-4498, 2010.
[24] G. Berkooz, P. Holmes, and J. Lumley, "The Proper Orthogonal Decomposition in the Analysis of Turbulent Flows", *Annual Review of Fluid Mechanics*, Vol. **25**, No. 1, pp. 539-575, 1993.
[25] N. De Lucca, S. Gordeyev and E.J. Jumper, "In-flight Aero Optics of Turrets", *Journal of Optical Engineering*, Vol. **52**, No. 7, 071408, 2013.